Robotics: Science and Systems 2024
Delft, Netherlands, July 15-July 19, 2024

Optimal Non-Redundant Manipulator Surface Coverage with Rank-Deficient Manipulability Constraints

Tong Yang*, Jaime Valls Miro†‡§, Li Huang¶, Yue Wang*, and Rong Xiong*
*Robotics Laboratory, Zhejiang University, P.R. China
Email: {tong.yang, ywang24, rxiong}@zju.edu.cn
†AZTI Foundation, Sukarrieta, Spain
‡IKERBASQUE, Basque Foundation for Science, Bilbao, Spain
§Robotics Institute, University of Technology Sydney, NSW, Australia.
Email: jvalls@azti.es
¶Institute of Advanced Digital Technologies and Instrumentation, Zhejiang University, P.R. China.
Email: li.huang@zju.edu.cn

***Abstract*—A generalised solver for the manipulator non-revisiting coverage path planning (NCPP) problem is proposed in this paper. Nonlinear manipulator kinematics and the imposition of task-specific constraints dictate that applying conventional coverage path planning (CPP) solutions based on 2D template matching or cellular decomposition schemes on the target surface invariably results in the robot path being an alternating sequence of task-executing movements and reconfiguring movements. Likewise, coverage paths designed directly in joint-space cannot ensure task-space non-repetitiveness. More recent state-of-the-art works have proposed finite-step optimal NCPP solutions where singularities are however expressly disregarded. Directly incorporating singular configurations violates the local bijectivity and finite-to-one property in the kinematic mapping, and cannot be properly modelled within existing schemes. This work leverages "valid" singularities, those that exhibit sufficient manoeuvrability in suitable dimensions to allow continuation of the tracking motion, thus further reducing the number of posture reconfigurations. The scheme assumes a generic representation of surfaces as discrete meshes, symbolising a null probability to locate the points corresponding to valid but singular inverse kinematic configurations, and constructs a practical method to traverse a singularity without explicitly calculating it. Simulated and realistic experiments are carried out where the suitability of the scheme to reduce posture reconfigurations and achieve continuous coverage motions are compared with existing methods. Three scenarios have been examined whereby the planner is able to fulfil motions without discontinuities in all instances.**

I. Introduction

Complete examination of an object's surface with a non-redundant manipulator is embodied in automated tasks such as polishing [27], deburring [31], painting [13] [26] or surface inspection [19] [14]. The need for non-repetitive coverage path planning (NCPP) is paramount to avoid retracing in such scenarios, yet the kinematic relationship of a typical rigid body manipulator makes mapping between a desired task-space path and the arm's joint-space non-bijective, which in effect drives coverage paths to be traditionally carried out in the task domain [20] [34]. The result is often undesirable arm reconfigurations that break up the planned continuity of the end-effector (EE) path [11].

In further pursuing motions where the manipulator seeks to minimise the number of imposed reconfigurations, a global optimal cellular decomposition solution in joint-space has been proposed that assembles joint-space partitions with minimum sets [33] [35]. A simple case is illustrated in Fig. 1(a). Points on the surface can be reached with a variety of robot poses, which belong to a finite set of configurations ("elbow-up", "shoulder-left", etc). The four solid colour regions shown illustrate the disjoint sets of poses reachable as a continuous collection with each configuration. As such, the kinematic relationship between a connected joint-space set and its task-space EE pose set is injective, and any arbitrary geometric coverage path that may be adopted within the region is guaranteed to be continuous in joint and path spaces.

To find the best visiting path for full object coverage, a topological graph is created whose elemental cells are drawn from intersecting the continuous configuration regions (three cells emerge in this case). A cellular decomposition process ensues that splits and merges subsets within cells, effectively transforming the process into that of optimally colouring all points in the graph with one of the possible colours in a way that a minimum set is attained, which equates to a path with the least number of EE lift-offs. The adoption of any coverage path inside each of the coloured sub-regions will result in a global path with maximum joint continuity [36].

Existing solutions to the non-redundant NCPP problem have purposely disregarded singular configurations [33] and their nearby ill-conditioned configurations [15]. This significantly reduces the problem difficulty in that kinematics between joint- and desired task-space poses becomes locally bijective, thus operating in a finite-to-one scheme. This approach however removes the associated singular connectivity. In general, there may exist surface points that are coverable by valid singular configurations deemed suitable for the coverage task,

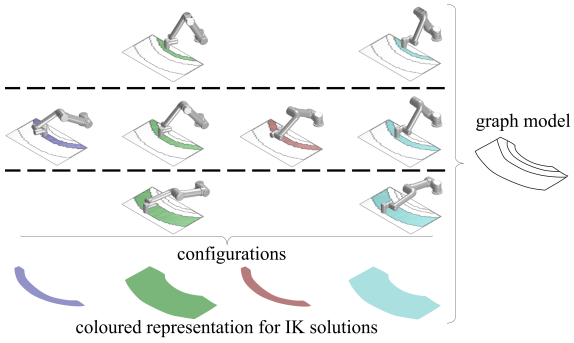

(a) NCPP, with full-rank manipulability constraints

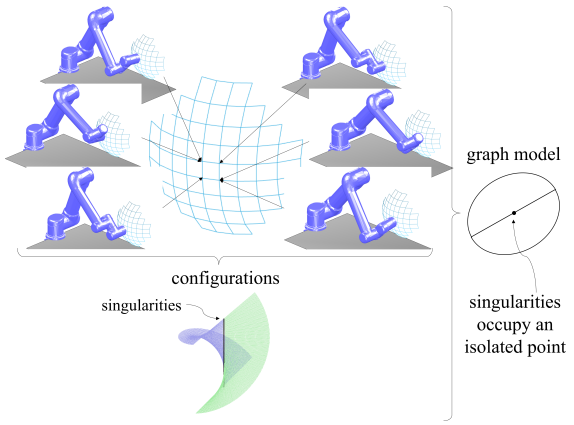

(b) Singularity-assisted NCPP, with rank-deficient manipulability constraints

Fig. 1. The proposed SNCPP over the standard NCPP solver. The optimal non-redundant NCPP problem seeks to cover all the reachable points on the surface of an object with minimal manipulator lift-offs. (a) Prior works ignore singularities, making the manipulator kinematic mapping for the desired EE poses finite-to-one and locally bijective. Visually, this is like a direct superimposition of paintable colours onto the graph. (b) In contrast, this work considers singularities. This is proven to improve joint-space connectivity, reducing manipulator travelling. Yet the introduction of singularities breaks local bijectivity and brings new challenges associated with infinite-to-one kinematic mappings. For more details about the figure refer to the text.

conditioned on arm kinematics, the object's pose and the path geometry. This is illustrated by the black line depicted bridging the configurations in Fig. 1(b). When they exist, these valid singularities belong to a border set bridging previously non-singular disconnectable sub-regions, and introduce a pose transition where the EE does not depart the objects's surface.

This, however, breaks the local bijectivity of the kinematic mapping, and imposes an infinite-to-one mapping on those surface points, which has not been considered in existing NCPP graph solvers. The task of finding NCPP-suitable singularities is non-trivial, and is only made harder by the discrete set of mesh points that generally make up an object's surface representation: there is zero probability of identifying a singularity by calculating the Inverse Kinematics (IK) in the limited set of surface points. Existing cellular decomposition schemes are thus not equipped to exploit this advantageous planning proposition, and a suitable approach must be found able to, simultaneously a) identify non-singular continuity among configurations in the joint-space, and b) asymptotically explore the existence–or absence–of suitable singularities between disjoint sets of valid non-singular configurations. By appropriately incorporating novel solutions to these two challenges within the framework of an existing NCPP topological graph solver, an improved manipulator motion can be proven guaranteed and finitely solvable.

The novel contributions in this work can be listed as:

1) Generalisation to the NCPP problem whereby valid singularities given by rank-deficient manipulability-related constraints can be capitalised on to improve continuity in the resulting joint motions. The resulting scheme is termed *Singularity-assisted Non-revisiting Coverage Path Planning* (SNCPP).
2) Proof of the topological equivalence between singularities and cells, so that singularities are proven to be replaceable by cells–an established structure to solve the NCPP problem. This process transforms the SNCPP problem into a form amenable to be solved by existing graph solvers.
3) Proof of the ability of the scheme to leverage singular IK configurations in an implicit form, without the need for an explicit calculation, thus overcoming the challenge of incorrectly identifying joint-space non-singular connectivity on discrete surfaces.

The remainder of this paper is organised as follows. Section II reviews existing literature. Section III sets the SNCPP problem scope. Section IV briefly reviews the current maximal continuity graph painting solver. Section V formally analyses relevant aspects of manipulator mobility around singularities. The graph model is then generalised to solve the SNCPP problem on analytic (Section VI) and discrete (Section VII and Section VIII) surfaces. Experimental results from both simulation and real-world experiments are then collected in Section IX, with Final concluding remarks gathered in Section X.

II. Related Works

The manipulator non-revisiting coverage path planning (NCPP) is an integrated body of the classic coverage path planning (CPP) problem [5], manipulator kinematics, and special designing frameworks guaranteeing non-repetitive coverage [32].

Early work on the CPP tasks has mainly adopted a hierarchical cellular decomposition structure for path generation. The target region is first partitioned into simple and easily handled cells [23] [1], which can then be traced with low level geometric coverage paths generated within each cell [2]. Cellular decomposition approaches address varying optimality conditions, e.g. regularity of cells [3], applicability to various kinds of target surfaces [1] or the division of the coverage task for multi-robot parallel operation [12]. Likewise, differing aspects of coverage performance have been considered for geometric coverage path generation, such as time-to-completion, energy minimisation [30] [18], coverage rate

maximisation [29], uniformity [36], path smoothness [7] or coverage path updates when unknown obstacles appear [21].

When it comes to the specific object surface CPP with manipulators, the most utilised coverage algorithms are directly drawn in the task-space of the object surface, homeomorphically deforming pre-patterned coverage paths into task-space target regions [1]. This approach is sometimes also referred to as tool coverage path planning, rather than manipulator coverage path planning. Or, as before, partitioning the surface into cells and designing coverage path within each cell through these same planar fitting schemes. However, such coverage paths do not consider manipulator kinematics; the EE is effectively regarded as the "robot", thus ignoring any manipulator-related constraints, and directly operating in the target region–whether it be the object surface [17], a shell of 3D points equidistant from the object surface [6] or the most generic form of a two-dimensional manifold of desired EE poses–for coverage. Hence they are only applicable when the object surface is near-flat and suitably contained in size to be strategically placed within reach in the manipulator workspace [16]. Otherwise, the EE is inevitably lifted off the surface, leading to undesirable manipulator pose reconfigurations and coverage task discontinuities. A relatively dense set of key points to be visited can also be placed strategically on the surface for the task at hand, and the path searching problem is solved via e.g. the Generalised Travelling Salesmen Problem [10]. This is presented in a bush trimming setting for instance where reaching the desired manipulator postures for the correct cutting necessitated cumbersome rearrangement motions, and undesired non-cutting arm readjustment motions along the path [11].

It is arguable that for surface contact coverage tasks in particular, the cost incurred in joint discontinuities significantly outweighs other metrics, e.g. by switching between differing geometric paths such as boustrophedon [4] and spiral as proposed in [7], or when undesirable transitions between position and force/torque control [8] [22] [25] become unavoidable. Redundant manipulators might be used to partly mitigate the problem of frequent coverage interruption [9]. However, in complex NCPP scenarios, redundant kinematics still cannot guarantee the elimination of discontinuities.

More recently, a new scheme has been proposed [32], where the manipulator NCPP was guaranteed to be solved with minimum discontinuities. This was reached by constructing and enumeratively solving a topological graph of continuous configuration cells. It was proven suitable to any generic multiply-connected cells, and optimally solved in finite steps [33] [37]. However, the authors purposely overlooked the complex case of singular configurations which can bridge different sets of non-singular configurations. This is so even though singular configurations are prevalent and problematic in most manipulator scenarios beyond the redundant case. In this instance. an over-actuated manipulator will exhibit an infinite number of alternate non-singular configurations to visit during an NCPP motion so that singularity avoidance algorithms for redundant kinematic systems can be effectively used to locally bypass singularities [28]. For the rest–the vast majority of arms–the presence of singularities in a non-redundant NCPP context essentially render the manipulator under-actuated at these configurations. The motivation of this work is observing the usefulness of these singularities and leveraging them given a manipulation task that does not require manoeuvrability along all dimensions (diagnosed by rank degeneration in the Jacobian matrix). The scheme proposed in this paper is thus able to properly incorporate valid singularities for NCCP, leading to further lift-off minimisation.

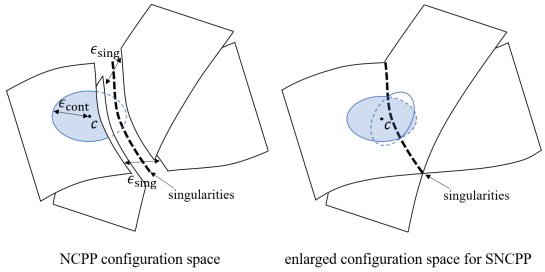

Fig. 2. Difference between NCPP and SNCPP. Left: consideration of full-rank manipulability-related constraints leads to the dismissal of singularities, ensuring a locally bijective kinematic mapping between each connected joint-space sub-set and task-space [33]. Surrounding ill-conditioned configurations are also removed, forming a non-zero gap between connected joint-space sub-sets, denoted as ϵ_{sing}. Right: by regarding valid singularities when they exist, distinct non-singular configuration sub-sets are connected. This introduces the potential to traverse across sub-sets without discontinuity but sacrifices the property of local kinematic bijectivity, calling for a new mechanism to handle singularities.

III. Problem Statement

Given a manipulator and a work-cell where the geometry of any obstacle in the environment is known and invariant, let the surface of the object be denoted as M. For each surface point, the EE pose required to visit that point is uniquely determined, hence the task-space sub-set to be non-repetitively covered forms a 2-dimensional manifold. For simplicity, we do not literally differentiate between a surface point and the unique EE pose required to visit this point. The manipulator is assumed kinematically non-redundant, meaning that for each surface point, there exists at most a finite number of non-singular inverse kinematic configurations. Among these configurations, only a finite number are valid–meaning they satisfy all the task-specified constraints (e.g. collision-free, being able to exert some pre-specified forces, etc.) across all dimensions, along with other task-specific constraints.

The *Non-revisiting Coverage Path Planning* (NCPP) problem is that of finding a sequence of valid non-singular configurations, guiding the tool trajectory to visit all desired EE poses exactly once. Optimal NCPP solutions are defined as the resultant paths with a minimum number of coverage discontinuities. This problem has been proven solved [32] [33]. The *Singularity-assisted Non-revisiting Coverage Path Planning* (SNCPP) problem generalises NCPP by allowing for manipulability-related constraints to be rank-deficient. In this scenario, singular configurations along with their neighbouring

ill-conditioned configurations may be valid. This introduces additional joint-space connectivity, potentially enhancing execution performance with fewer discontinuities compared to the optimal NCPP solution. The distinct two schemes are visually depicted by the example given in Fig. 2.

IV. NCPP Preliminaries

This section recounts existing notations and formulations for finding non-redundant non-revisiting manipulator coverage paths with a minimum number of EE lift-offs, or discontinuities.

The kinematic relation of a robotic manipulator is written as:

$$\mathbf{x} = \mathbf{f}(\mathbf{q}) \tag{1}$$

where $\mathbf{f}$ is a differentiable nonlinear vector function whose structure and parameters are assumed to be known for any given manipulator. The above equation can be differentiated with respect to time as:

$$\dot{\mathbf{x}} = \mathbf{J}(\mathbf{q})\dot{\mathbf{q}} \tag{2}$$

where $\mathbf{q}$ is the $(n \times 1)$ vector of manipulator joint variables, $\mathbf{x}$ is the $(m \times 1)$ vector of task variables, and $\mathbf{J}$ is the $(m \times n)$ configuration dependent Jacobian matrix (also known as $\partial\mathbf{f}/\partial\mathbf{q}$). An upper dot denotes time derivative. And we will denote a single configuration $c = \mathbf{q}$.

Definition 1. *(Manipulability) For a joint configuration c, manipulability $W(c)$ is defined as [38]:*

$$W(c) = \sqrt{\det(\boldsymbol{J}\boldsymbol{J}^\top)} \tag{3}$$

At a singularity, $W(c) = 0$.

Definition 2. *(Valid Configuration) A valid configuration c satisfies the following:*

1) *It is collision-free.*
2) *Point contact between the surface and the EE is established.*
3) *A set of task-specific constraints represented by strict inequalities are satisfied. The k-th constraint can be generically written as:*

$$F_k(c) > \delta_k \tag{4}$$

where $\{F_k\}$ are assumed to be joint-space continuous functions and δ_k is a set threshold.

The validation of constraints may be implicit. For instance, for a task where the EE is required to horizontally exert a force greater than 5N, the constraint is verified by computing the force on each joint. It is deemed satisfied if all joints adhere to their respective maximum force limits.

Definition 3. *(Configuration Space) The set of all valid non-singular configurations is referred to as configuration space, denoted by $\mathscr{C}$.*

Definition 4. *(Colour) A colour is defined as the index of a path-connected sub-set of valid non-singular configurations in the configuration space $\mathscr{C}$. Hence $\mathscr{C}$ is divided into disjoint sets,*

$$\mathscr{C} = \mathscr{C}_1 \sqcup \mathscr{C}_2 \sqcup \cdots \mathscr{C}_L \tag{5}$$

The colour of the configurations in $\mathscr{C}_i$ is labelled as i. Besides indexing by numbers, colours may also be referred to as actual words, "red", "green", "blue", etc.

Please note that for the sake of symbolic consistency, in the algorithmic sections, even when a singular configuration may be valid, they remain excluded from $\mathscr{C}$.

Definition 5. *(Cell) A cell V_i (where i is its index) is a maximal path-connected set*[1] *of surface points such that*

1) *Each point corresponds to a finite number of IK configurations.*
2) *For any two points, their IK solutions are pairwise continuous, i.e.,*

$$\begin{aligned} &\forall \epsilon > 0,\ \exists \delta > 0, \\ &\quad \forall m_1,\ m_2 \in V_i,\ \textit{s.t.}\parallel m_1 - m_2 \parallel < \delta, \\ &\quad\quad \forall c_1 \in \mathrm{IK}(m_1),\ \exists c_2 \in \mathrm{IK}(m_2),\ d(c_1, c_2) < \epsilon \end{aligned} \tag{6}$$

where $d(\cdot,\cdot)$ is the joint-space distance.

The constraints for configuration validity $\{F_k\}$ are all strict inequalities. As such, each cell is an open set.

Each coverable surface point is associated with a finite set of colours, representing the colours corresponding to its valid inverse kinematic configurations. By definition, all points within a cell correspond to the same set of colours, the possible colours of the cell.

Definition 6. *(Edge) An edge E_i is a maximal connected curve of surface points e shared by the boundary of two cells V_j and V_k, i.e.,*

$$\begin{aligned} E_i = E_i(V_j, V_k) = \{e | \forall \epsilon > 0, \exists m, m' \in B(e, \epsilon), \\ m \in V_j, m' \in V_k, j \neq k\} \end{aligned} \tag{7}$$

where $B(e, \epsilon)$ is an open ball centred at e with radius ϵ.

A topological graph is defined as the group of cells $\{V_i\}$ equipped with the adjacency of cells specified by edges $\{E_j\}$.

It has been observed that in the presence of full-rank manipulability constraints, the non-redundant kinematic relationship between configuration space and surface (i.e., the desired 2D manifold of EE poses) is locally bijective. This has been visually interpreted as the equivalence between painting a point in the graph and assigning a valid inverse kinematic configuration to cover this point. Therefore, the NCPP problem has been modelled in a purely abstract form, painting the whole graph with a minimum number of coloured regions. For full details of the enumerative solving procedure see [32] [33].

[1]The term "path-connected" means every two surface points in the same cell yield a curve connecting them which is fully in the cell. The term "maximal" means the cell cannot include any other surface points. All path-connected surface points outside the cell do not satisfy the specified conditions.

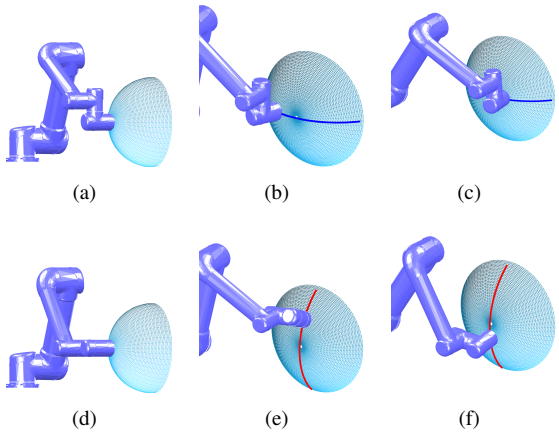

Fig. 3. Illustration of the admissible tool motion on an idealised surface (light blue) at two singular configurations for the UR5, a typical example of a six-revolute joints manipulator. The robot has three types of singularities and two examples of wrist singularities are provided where axes 2 (shoulder), 3 (elbow), 4 (the first wrist joint), and 6 (the last wrist joint) are parallel. (a) Wrist singularity with wrist link 5 perpendicular to the ground. (b)(c) EE can only move horizontally on the surface, shown as a blue curve. No joint can control the pitch angle. (d) Wrist singularity with wrist link 5 parallel to the ground. (e)(f) EE can only move vertically on the surface, shown as a red curve. No joint can control the yaw angle.

V. SNCPP: Continuous Surfaces

The distinct characteristics of manipulator configurations in the vicinity of singularities that give rise to the SNCPP solution proposed in this paper are hereby formally analysed.

A. Mobility under Rank-Deficient Manipulability Metrics

In the SNCPP problem, manipulability-related constraints are no longer required to be of full-rank. Instead, they are assumed to be rank-deficient. This paper employs the translational manipulability [39] of a 6-DoF serial manipulator for easy illustration, expressed by

$$F_1(c) = \sqrt{\det(\bar{\mathbf{J}}\bar{\mathbf{J}}^\top)} \tag{8}$$

where $\bar{\mathbf{J}}$ is the top three rows of the Jacobian $\mathbf{J}$. In the remaining paper, we will still refer to $F_k(c)$ for generality.

Definition 7. *(Assistive Point) A surface point coverable with a valid singular configuration is denoted as an assistive point.*

A point covered by a singular configuration may also be coverable by a finite set of valid non-singular configurations.

B. Admissible Direction to Visit Valid Singularities

A singularity impedes omni-directional movements of the EE on the 2-dimensional task-space manifold. Having lost 1 DoF, a 1-dimensional null-space simultaneously appears. However, effortless motion along this null-space dimension is typically discouraged in a coverage task (for illustration, in a polishing task this would equate to keeping the tool statically on the same surface point, which could potentially damage the surface). Consequently, losing 1 DoF implies that only motion along the remaining 1D manifold is permitted [2]. The admissible motion at a singularity for the useful case when 1 DoF is lost [24] must thus follow a path on a plane, as proved next. This is an important observation that will be of relevance to be able to efficiently traverse through singularities. Please refer to Fig. 3 for example with the kinematics of a UR5.

Theorem 8. *Given a valid singular configuration which has lost 1 DoF, the movable end-effector direction along the surface is unique. In other words, all tool paths visiting an assistive point with a valid singular configuration have the same unit tangent direction (subject to reversal).*

Proof: The explicit formula for the tool path is given by dimension decomposition. Applying singular value decomposition to $\mathbf{J}$

$$\mathbf{J} = \mathbf{U}\mathbf{\Sigma}\mathbf{V}^\top \tag{9}$$

where $\mathbf{U}$, $\mathbf{V}$ are orthonormal matrices. The rank of $\mathbf{\Sigma}$ is 5 because the configuration is one-DoF singular, so we denote

$$\mathbf{\Sigma} = \mathrm{diag}(\sigma_1, \cdots, \sigma_5, 0),\ \ \sigma_1 > \cdots > \sigma_5 > 0 \tag{10}$$

Early work [24] has named the *accessible space coordinates* $\hat{\dot{\mathbf{x}}}$ and the *modified joint-space velocity* $\hat{\dot{\mathbf{q}}}$ as

$$\hat{\dot{\mathbf{x}}} = \mathbf{U}^\top \dot{\mathbf{x}} \tag{11}$$

$$\hat{\dot{\mathbf{q}}} = \mathbf{V}^\top \dot{\mathbf{q}} \tag{12}$$

Then the instant tool motion (i.e., the tool velocity) is executable if and only if it occupies the effective rows in the modified joint space, which is referred to as being restricted in a sub-manifold:

$$\dot{\mathbf{x}} \text{ is executable } \Leftrightarrow \mathbf{x} \text{ satisfies } \hat{\dot{x}}_6 = 0 \tag{13}$$

This imposes an additional one-dimensional constraint on the motion direction of the tool on the surface. To reveal this, denoting

$$\dot{\mathbf{q}}^- \triangleq \mathbf{V}[\hat{\dot{q}}_1, \cdots, \hat{\dot{q}}_5, 0]^\top,\ \ \dot{\mathbf{q}}^\perp \triangleq \mathbf{V}[0, \cdots, 0, \hat{\dot{q}}_6]^\top \tag{14}$$

the first 5-DoF modified joint space motion $\dot{\mathbf{q}}^-$ is effective, performing the admissible (one-dimensional) tool motion, and the last velocity component $\dot{\mathbf{q}}^\perp$ performs the null motion. ■

It is noteworthy that whilst the EE may have zero velocity along the degenerated dimension, it may have non-zero acceleration. In other words, the tangent of the EE trace at the assistive point must align with the admissible direction, whilst it can have non-zero curvature.

VI. Generalisation of the Graph Painting Model

In this section, the SNCPP problem of an object's surface with analytic expressions is formally modelled as a topological graph, and optimally solved with the proposed algorithm. It will give rise to the central difficulty in seamlessly incorporating singularities into the existing cell-edge graph structure.

[2]Evidently, surrendering another DoF means no EE motion is permitted.

A. Traversing Assistive Points

The state-of-the-art (SOTA) topological graph framework to solve the NCPP problem is unable to consider singularities, given that the region that assistive points occupy is a zero area, meaning that the spatial distribution of assistive points cannot be represented as an open region. They are a point or a curve of points, which have not been modelled into the graph. One strategy is representing the assistive point as a cell instead, as shown by the dotted circle in Fig. 4. It remains to be proven, however, whether solving the modified topological graph can yield the optimal solution of the original graph. Should a singularity be visited, yet not the assistive point but a cell region be marked as visited, the surface points coverable by each possible colour could still be covered without an EE lift-off. This is described by the following theorem.

Theorem 9. *(Location of Assistive Point) Any assistive point is located at the reachable boundary of exactly two colours.*

Proof: Let the assistive point be denoted as s, and the singular configuration visiting s be denoted as c_s. The two colours connectable by the singular configuration are indexed as i and j. Given **Theorem** 8, there exists a joint-space motion c_γ whose task-space tool curve γ visits s in the admissible direction. Hence c_γ is the continuous motion in $\mathscr{C}_i$ that connects to c_s,

$$\begin{aligned} \forall \epsilon > 0,\ \exists m \in \gamma \cap B(s,\epsilon),\ \text{s.t.} \\ \exists c \in \mathrm{IK}(m),\ c \in \mathscr{C}_i \end{aligned} \tag{15}$$

Since $c_s \notin \mathscr{C}_i$, s is on the reachable boundary of colour i. The same is true for colour j.

Next, it is proven that s is not located at the boundary of other colours. Let C_s be the set of non-singular configurations that cover s. If C_s is empty, the theorem is proven. Otherwise, assuming that s can also be visited by N valid non-singular configurations,

$$C_s = \{c_1, \cdots, c_N\} \tag{16}$$

every $c_j \in \mathscr{C}_s$ must satisfy all constraints,

$$F_k(c_j) > \delta_k,\ \forall k,\ \forall j = 1, \cdots, N \tag{17}$$

Given that all constraints $\{F_k\}$ are strict inequalities and continuously defined, there exists a joint-space open neighbourhood U_j where all constraints still hold,

$$\begin{aligned} F_k(c) > \delta_k + \frac{1}{2}(F_k(c_j) - \delta_k) > \delta_k, \\ \forall j,\ \exists U_j,\ \forall k,\ \forall c \in U_j \end{aligned} \tag{18}$$

Since the manipulator forward kinematics (FK) is locally homeomorphic in the vicinity of every non-singular configuration, $\mathrm{FK}(U_j)$ is also an open set,

$$c_j \in U_j \Rightarrow s \in \mathrm{FK}(U_j), \forall j = 1, \cdots, N \tag{19}$$

and so must be the intersecting area,

$$s \in A_s \triangleq \cap_{j=1}^{N}(\mathrm{FK}(U_j)),\ \forall j = 1, \cdots, N \tag{20}$$

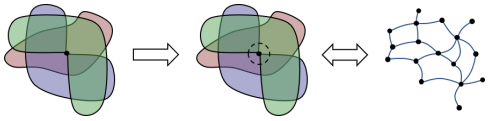

Fig. 4. Illustration of **Theorem 9**. Wherever an assistive point of two colours exists, an assistive cell can be constructed in its vicinity which acts equivalently to the singularity: it maintains the ability to bridge the two colours whilst not affecting the connectedness of any other colour.

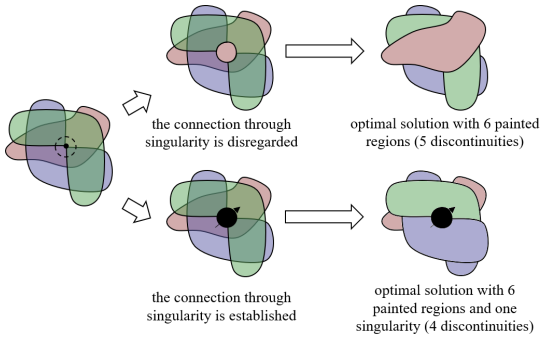

Fig. 5. Illustration of enumeratively solving a graph with a singularity. Upper branch: disregarding the singularity, a minimum of 6 regions are required to fill the whole graph, which is the optimal solution for the normal NCPP problem. Lower branch: introducing the singularity, the central blue and green regions are connected, leading to a reduced number of regions, 5, a better solution.

Recalling that N is a finite set, the finite intersecting of open regions must thus be a non-zero area. For any colour covering s, it can also cover the whole area A_s. So let $B(s,\delta) \subset A_s$ be an open ball entirely contained within A_s, then δ is a non-zero clearance between s and the reachable boundary of any other colour. This means that s is not located at the boundary of other colours. ■

When assistive points form a curve on the surface, **Theorem 9** is still applicable. In summary, an *assistive cell* can always exists, as defined by:

Definition 10. *(Assistive Cell) For a connected set of assistive points, the assistive cell is a minimal open region that encloses the assistive points.*

In the Fig. 4 example, the two colours connectable by visiting the singularity (blue and green) cannot fully cover all points in the cell, so the possible colours (only one here, $\{red\}$) will be set as the colour of the non-singular configurations at the assistive point. There could be more in general.

B. Graph Solver

After the topological graph has been constructed, with the aid of the assistive cells, connectivity between the two colours of a singularity is binary, either connecting or disconnecting. See Fig. 5 for an illustration of the branching in the enumerative processes. If the two colours (green and blue in this case) are assigned to be connected by visiting the singularity, the assistive cell is marked as "filled". This prevents other colours from repetitively visiting the assistive point. After the graph is fully painted, the number of painted regions is reduced

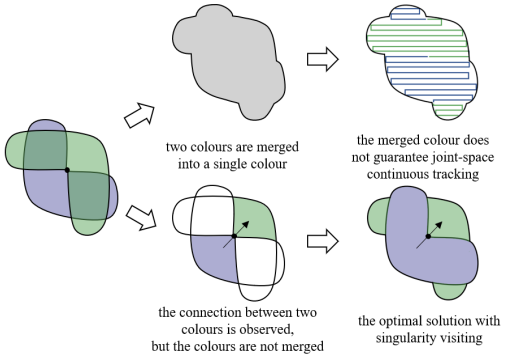

Fig. 6. Difference between observing connectivity by singularity visiting and merging colours connectable by singularity visiting. The resulting geometric coverage path generated in the coverable region of the merged colour cannot be continuously tracked in joint-space (top branch). Four motion segments with three reconfiguration motions are required. The preferred graph construction calls for the correct differentiation of colours whilst correctly observing the connectivity through a singularity, ending up with 2 reconfigurations.

by 1 if both a blue region and a green region are adjacent to the assistive cell. If the connection is disregarded, it is equivalent to regarding the assistive cell as an ordinary cell. Either way, the remaining part of the graph does not have any undetermined connectivity derived from singularities and can be subsequently optimally solved as a regular graph [33].

VII. SNCPP: Discrete Surfaces

Unlike the aforementioned SNCPP solution on a continuum, connectivity between two configurations in a discrete surface setting is recognised by their joint-space distance. In doing so, two configurations that lie on opposite sides of a singularity, therefore belonging to different colours in the analytic case, may be recognised as a single colour in the discrete case. This is misleading in that a geometric path between the two merged configurations will appear as continuous in joint space, even though they are unconnectable everywhere except at the singularity. See Fig. 6 for an illustrative example.

Moreover, it is often the case that a small tool displacement near a singularity requires long joint-space detours, however continuous without visiting the singularity. This indicates that two continuous but near-singular configurations (i.e., having the same colour) may easily develop into large joint-space displacements. On purely joint metrics they would likely be wrongly recognised as disconnected configurations, and labelled with different colours. Therefore, a specific mechanism to handle discrete representations for the SNCPP beyond the continuous analysis is needed to be able to apply the proposed graph modelling solver.

A. Further Definitions

Some further definitions are required to formally describe the asymptotic modelling and solving of the NCPP problem on discrete surfaces. See Fig. 7 for the conceptual illustration of symbols. Let the set of surface points M be assumed finite,

$$M = \{m_1, \cdots, m_N\} \tag{21}$$

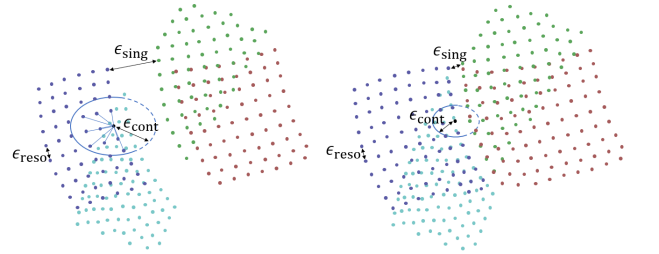

Fig. 7. Physical meaning of symbols. NCPP (left) and SNCPP (right).

all of which have only non-singular IK solutions $\{c_{m_i j}\}_{j=1}^{K_i}$, where K_i is the number of IK solutions. Thus the configuration space $\mathscr{C}_{\text{D}}$ is also a finite set:

$$\mathscr{C}_{\text{D}} = \{c_{m_i j},\ j = 1, \cdots, K_i,\ i = 1, \cdots, N\} \tag{22}$$

Remark 11. *Colour assignment to configurations in the discrete case is the same as in the continuum surface case, i.e., two configurations are of the same colour if they can be non-singularly connected without EE lift-off, regardless of how their continuity is discretely recognised. Thus decomposition based on colours for $\mathscr{C}$ in Eqn. (5) remains valid. The set of IK configurations captured from discrete surfaces belonging to colour i is denoted as $\mathscr{C}_{\text{D}i}$.*

Definition 12. *(Discrete Task-Space Adjacency) The adjacency between point m_i and m_j is denoted as $m_i \leftrightarrow m_j$, determined by the input data. For instance, two vertices of a mesh are adjacent only when they are the endpoint of an edge.*

Definition 13. *(Discrete Joint-Space Continuity) The joint-space continuity of two configurations is judged by a parameter ϵ_{cont}, i.e.,*

$$c_1, c_2 \text{ are continuous} \Leftrightarrow \begin{cases} \text{FK}(c_1) \leftrightarrow \text{FK}(c_2), \\ d(c_1, c_2) < \epsilon_{\text{cont}} \end{cases} \tag{23}$$

where $d(\cdot, \cdot)$ is the joint-space distance.

Definition 14. *(Discretisation Resolution) ϵ_{reso} is defined as the maximum distance between the adjacent configurations belonging to the same colour,*

$$\epsilon_{\text{reso}} = \max_{\substack{c, c' \in \mathscr{C}_{\text{D}i}, \\ \text{FK}(c) \leftrightarrow \text{FK}(c'), \forall i}} d(c, c') \tag{24}$$

ϵ_{reso} quantifies how densely the continuous joint-space is discretised into distant configurations.

Definition 15. *(Singular Discretisation Resolution) ϵ_{sing} is defined as the minimum distance between two adjacent configurations belonging to different colours,*

$$\epsilon_{\text{sing}} = \min_{\substack{c \in \mathscr{C}_{\text{D}i}, c' \in \mathscr{C}_{\text{D}j}, \\ \text{FK}(c) \leftrightarrow \text{FK}(c'), i \neq j, \forall i, j}} d(c, c') \tag{25}$$

ϵ_{sing} quantifies how far apart the non-singular configurations are, which cannot be connected without visiting singularity.

B. Asymptotic Parameter Variations and Valid ϵ_{cont}

This subsection provides a proof of a discouraging result: For a high-resolution discrete surface aiming to obtain more configurations near potentially existing assistive points (even without the knowledge of their locations) and achieve a high-resolution optimal SNCPP solution, a valid choice for ϵ_{cont} does not exist.

Given a surface mesh constructed from sensed data (e.g. an RGBD camera), ϵ_{reso} and ϵ_{sing} would end up with some fixed values, and only ϵ_{cont} can be arbitrarily set by the coverage path planner. The following relations between parameters have to be satisfied:

1) $\epsilon_{\text{reso}} < \epsilon_{\text{cont}}$. Otherwise, non-singularly connectable IK configurations would be recognised as disconnectable and be labelled as different colours.
2) $\epsilon_{\text{cont}} < \epsilon_{\text{sing}}$. Otherwise, configurations near a singularity, which are non-singularly disconnectable, would be recognised as connectable and be labelled as the same colour.

From 1) and 2), $\epsilon_{\text{reso}} < \epsilon_{\text{sing}}$ is implicitly required. However, it is proven next that this relation does not hold as the discrete surface resolution increases.

Lemma 16. *As the surface resolution grows,* $\epsilon_{\text{sing}} \to 0$.

Proof: (See Fig. 8(a) for illustration). Let the assistive point be denoted s, and the two colours connectable by visiting singular configuration be indexed i and j. By **Theorem** 8, there exists a joint-space motion c_γ whose task-space tool curve γ visits s in the admissible direction. For an arbitrarily small threshold $\epsilon > 0$, there exist two points m_1 and m_2 on γ whose IK in c_γ have different colours, i.e.,

$$\begin{aligned} \forall \epsilon > 0,\ \exists \delta > 0,\ \forall m_1,\ m_2 \in \gamma \subset B(s,\delta), \\ \exists c_1 \in \mathrm{IK}(m_1) \cap \mathscr{C}_i,\ c_2 \in \mathrm{IK}(m_2) \cap \mathscr{C}_j, \\ d(c_1, c_2) < \frac{1}{2}\epsilon \end{aligned} \tag{26}$$

Since all constraints $\{F_k\}$ are given by strict inequalities, there exists a joint-space neighbourhood of m_1 where all constraints still hold,

$$\begin{aligned} \exists U(m_1),\ \forall m' \in U(m_1), \\ \exists c' \in \mathrm{IK}(m') \cap \mathscr{C}_i,\ d(c', c_1) < \frac{1}{4}\epsilon \end{aligned} \tag{27}$$

The same is also true for m_2

$$\begin{aligned} \exists U(m_2),\ \forall m'' \in U(m_2), \\ \exists c'' \in \mathrm{IK}(m'') \cap \mathscr{C}_j,\ d(c'', c_2) < \frac{1}{4}\epsilon \end{aligned} \tag{28}$$

Since $U(m_1)$ and $U(m_2)$ are non-empty open sets, they are of non-zero area. Hence with non-zero probability, two such points m_1 and m_2 on the surface can be recognised as adjacent, with a distance between their IK less than ϵ. In summary,

$$\begin{aligned} \forall \epsilon > 0,\ \exists U(m_1),\ U(m_2) \text{ as defined above} \\ \forall m' \in U(m_1),\ \forall m'' \in U(m_2), \\ \exists c' \in \mathrm{IK}(m') \cap \mathscr{C}_i,\ \exists c'' \in \mathrm{IK}(m'') \cap \mathscr{C}_j, \\ d(c', c'') < d(c', c_1) + d(c_1, c_2) + d(c_2, c'') \\ = \frac{1}{4}\epsilon + \frac{1}{2}\epsilon + \frac{1}{4}\epsilon = \epsilon \end{aligned} \tag{29}$$

Thus, with non-zero probability, m' and m'' are captured on the discrete surface, leading to the addition of c' and c'' to $\mathscr{C}_{\text{D}}$. Then by definition,

$$\begin{aligned} \epsilon_{\text{sing}} &\le \min_{c' \in \mathscr{C}_{\text{D}i}, c'' \in \mathscr{C}_{\text{D}j}} d(c', c'') \\ &\le d(c', c'') < \epsilon \end{aligned} \tag{30}$$

Hence ϵ_{sing} converges to 0 when increasing surface resolution. ■

In contrast to the result just presented, it is hereby proven that for arbitrarily fine surface meshes, ϵ_{reso} does not converge to zero. This is because of the non-flatness of the configuration space near singularities: With non-zero probability, two surface points near an assistive point can be captured, whose IK solutions belong to the same colour but have a non-zero joint-space distance.

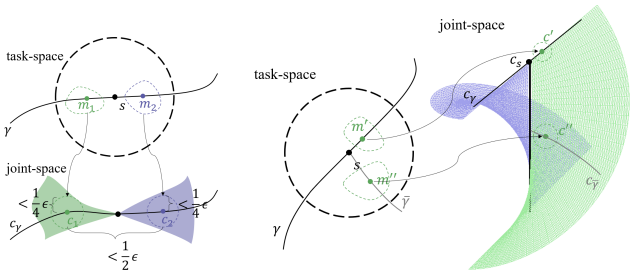

(a) **Lemma** 16 (b) **Lemma** 17

Fig. 8. Auxiliary figures.

Lemma 17. *As the surface resolution grows,* $\epsilon_{\text{reso}} \nrightarrow 0$.

Proof: See Fig. 8(b) for auxiliary illustration. Let the assistive point be denoted as s, the valid singular configuration covering s be c_s, and the colour connectable to c_s be indexed as i. By **Theorem** 8, there exists a joint-space continuous curve c_γ whose task-space tool curve γ visits s in the admissible direction. So for arbitrarily small threshold $\epsilon' > 0$ there exists a point m' on γ whose IK is close to the singularity,

$$\begin{aligned} \forall \epsilon' > 0,\ \exists \delta' > 0,\ \forall m' \in B(s,\delta') \cap \gamma, \\ \exists c' \in \mathrm{IK}(m') \cap \mathscr{C}_i,\ d(c', c_s) < \epsilon' \end{aligned} \tag{31}$$

And within an open ball centred at c' with radius $\frac{1}{2}\epsilon'$, the task-space image of the ball, $U(m')$, is a region surrounding

m',

$$\begin{aligned}&\exists U(m'),\ \forall \bar{m}' \in U(m'),\\ &\quad \exists \bar{c}' \in \mathrm{IK}(\bar{m}') \cap \mathscr{C}_i,\\ &\quad\quad d(\bar{c}', c_s) \leq d(\bar{c}', c') + d(c', c_s) < \frac{3}{2}\epsilon'\end{aligned} \tag{32}$$

and $U(m')$ is of non-zero area, because c' is non-singular.

Meanwhile, except the admissible direction, s cannot be visited along other directions. Let there be another task-space tool curve $\bar{\gamma}$ that visits s along another direction. The inability of continuously tracking $\bar{\gamma}$ means the existence of an ϵ'' gap between c_s and its nearby configurations:

$$\begin{aligned}&\exists \epsilon'' > 0,\ \forall \delta'' > 0,\ \exists m'' \in B(s, \delta'') \cap \bar{\gamma},\\ &\quad \exists c'' \in \mathrm{IK}(m'') \cap \mathscr{C}_i,\ d(c'', c_s) \geq \epsilon''\end{aligned} \tag{33}$$

And within an open ball centred at c'' with radius $\frac{1}{2}\epsilon''$, the task-space image of the ball, $U(m'')$, is a region surrounding m'',

$$\begin{aligned}&\exists U(m''),\ \forall \bar{m}'' \in U(m''),\\ &\quad \exists \bar{c}'' \in \mathrm{IK}(\bar{m}'') \cap \mathscr{C}_i,\\ &\quad\quad d(\bar{c}'', c_s) \geq d(c'', c_s) - d(\bar{c}'', c'') > \frac{1}{2}\epsilon''\end{aligned} \tag{34}$$

and $U(m'')$ is of non-zero area, because c'' is non-singular.

In this case, for any $\bar{\gamma}$, we can find a non-zero ϵ''. Fix ϵ'', we set

$$\epsilon' = \frac{1}{6}\epsilon'',\ \epsilon = \frac{1}{4}\epsilon'' \tag{35}$$

then with non-zero probability a discrete surface point $\bar{m}'$ is captured from the region $U(m')$ constructed above, and also, with non-zero probability $\bar{m}''$ is captured from $U(m'')$. By definition,

$$\begin{aligned}\epsilon_{\mathrm{reso}} \geq & \max_{\substack{\bar{c}', \bar{c}'' \in \mathscr{C}_{\mathrm{D}i} \\ \mathrm{FK}(\bar{c}') \leftrightarrow \mathrm{FK}(\bar{c}'')}} d(\bar{c}', \bar{c}'')\\ \geq & d(\bar{c}', \bar{c}'') \quad \text{(for the } \bar{c}' \text{ and } \bar{c}'' \text{ as defined above)}\\ \geq & d(\bar{c}'', c_s) - d(c_s, \bar{c}')\\ > & \frac{1}{2}\epsilon'' - \frac{3}{2}\epsilon' = \epsilon\end{aligned} \tag{36}$$

Hence ϵ_{reso} does not converge to 0 when increasing surface resolution. ∎

In summary, as the resolution of the input discrete surface increases, **Lemma** 16 and **Lemma** 17 yield

$$\begin{cases}\epsilon_{\mathrm{reso}} \to \epsilon^*_{\mathrm{reso}} > 0\\ \epsilon_{\mathrm{sing}} \to \epsilon^*_{\mathrm{sing}} = 0\end{cases} \Rightarrow \nexists \epsilon_{\mathrm{cont}} \text{ s.t. } \epsilon^*_{\mathrm{reso}} < \epsilon_{\mathrm{cont}} < \epsilon^*_{\mathrm{sing}} \tag{37}$$

Hence an additional strategy is necessary before the correct topological graph can be constructed on discrete surfaces.

VIII. Discrete SNCPP: Joint-Space Separation

A higher-level joint-space separation algorithm is presented to implicitly leverage singularities in a discrete SNCPP setting.

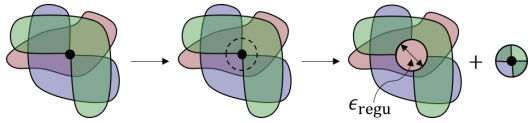

Fig. 9. Decomposition of the topological graph for singularity traversal.

A. Joint-Space Separation and Valid ϵ_{regu}

The problem of incorrect graph initialisation is fundamentally caused by the non-flatness of the configuration space near a singularity. Configurations close in task-space may be far in joint-space, leading to the convergence of ϵ_{sing} to zero whilst keeping ϵ_{reso} large. A joint-space separation is introduced to prevent ill-conditioned configurations from being mixed with other non-singular configurations. This separation is implemented by setting an auxiliary full-rank manipulability threshold ϵ_{regu}. See Fig. 9 for illustration.

The parameter ϵ_{regu} functions similarly to ϵ_{sing}, the difference being that ill-conditioned configurations are not removed. Besides, the user can arbitrarily set the volume indicating the extent of ill configurations that should be distinguished. After ill-conditioned configurations are excluded, the remaining configurations are all non-singular and locate on the flat part of the configuration space, close to the standard NCPP problem. In this case, ϵ_{sing} has a non-zero lower bound regardless of the surface resolution whilst ϵ_{reso} converges to zero with increasing surface resolution, allowing the user to choose the most appropriate ϵ_{cont}. In summary, after applying the joint-space separation strategy, $\epsilon^*_{\mathrm{sing}} > 0$ whilst $\epsilon^*_{\mathrm{reso}} = 0$, which allows the user to choose a valid ϵ_{cont}.

B. Optimal Setting of ϵ_{regu}

The exclusion of valid non-singular but ill-conditioned configurations, which are otherwise usable for coverage, results in the un-coverage of potentially continuously coverable surface regions. Clearly, the fewer ill-conditioned configurations excluded, the less difference between the coverable regions of each colour in the approximate normal NCPP problem and that of the same colour in the SNCPP problem. Therefore, the optimal solution is achieved when ϵ_{regu} is set as its smallest possible value. In the example in Fig. 10, when ϵ_{regu} is set to 0.14, some configurations with the colour blue and cyan are excluded, resulting in a large uncoverable hole in the centre of the circular surface. Whilst constructing the singular traversability between blue and cyan eventually leads to an optimal manipulator coverage path without discontinuity, the ϵ_{regu} has been set too large and a smaller value should be examined.

Fortunately, the setting of ϵ_{regu} being too small is easily identifiable: In the vicinity of a singularity, a configuration would be assigned a colour different from all its neighbours, covering a tiny cell, typically containing only one surface point. Simultaneously, another colour appears to cover the surrounding points excluding this particular one. Pictorially, the reachable boundaries of these two colours coincide. In the example in Fig. 10, when ϵ_{regu} is set to 0.05, four of the mesh

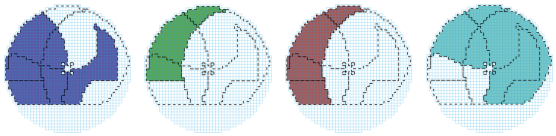

(a) $\epsilon_{\text{regu}} = 0.05$

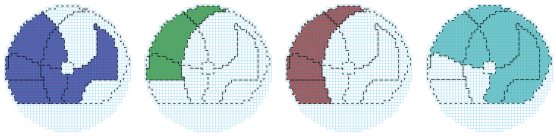

(b) $\epsilon_{\text{regu}} = 0.09$

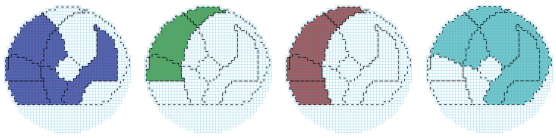

(c) $\epsilon_{\text{regu}} = 0.14$

Fig. 10. Illustration of different choices for parameter ϵ_{regu}.

vertices have IK configurations which cannot be recognised as connectable to other configurations by the given discrete continuity threshold. These lead to the creation of four one-vertex cells in the graph.

A practical binary search strategy is thus derived to find the optimal ϵ_{regu}: determine upper and lower bounds of the optimal ϵ_{regu}, and then proceed to search for the optimal value in a binary manner. An illustrative example is given by Fig. 10, where as indicated a value between 0.05 and 0.14 was the suggested boundary arrangement. Iteratively, the mid-point choice $\epsilon_{\text{regu}} = 0.09$ is then tested, and validated to still yield a correct graph representation, setting a new boundary. The new mid-point finer representation will be tested to assess whether it becomes a better choice, $\epsilon_{\text{regu}} = 0.07$ in this case, and taken as the new boundary if so. Finally, a situation is reached where further adjusting ϵ_{regu} to the middle value of the bounds does not change the graph representation, indicating the most suitable value for ϵ_{regu}, 0.09 in this example. It is worth noting that determining the most suitable ϵ_{regu} does not involve enumerative solving of the graph, hence the search strategy is efficient.

IX. Simulated and Real-world Validation

Simulated and real-world examinations of the proposed algorithm are presented to validate the scheme, including comparisons with competing schemes. The Universal Robots UR5 robot is used in all cases, except for the initial 2D toy study described next. To enforce the non-redundant kinematic setting, the last manipulator joint is kept locked. A coverage task emulating a finishing/polishing application is adopted throughout, whereby the EE (not shown in the figures) is a self-rotating unit with the rotating axis coincident with the last joint. The desired EE poses are thus perpendicular to the surface to be polished. As the proposed algorithm does not explicitly calculate singularity locations, various types of singularities do arise given the UR5 Kinematics, including shoulder, elbow and wrist singularities. However, given the assumption that the 6-th joint sits perpendicular when in contacts with the object surface (therefore cannot "intrude" the object whilst traversing singularities), only wrist singularities may be valid.

A. 2D Case Study

A simple 2-DoF case study is first described step-by-step to better illustrate the workings of the proposed algorithm, depicted in Fig. 11. Manipulator self-collision is neglected for simplicity. Both the continuous and discrete cases are presented. Let the target EE poses be a curve whose upper part is a half-ellipse, and the lower part a half-sphere, parameterised by

$$\alpha : [0, 2\pi) \to \mathbb{R}^2, \theta \mapsto (x(\theta), y(\theta)) \tag{38}$$

where

$$\begin{aligned} x(\theta) &= \sqrt{2}\cos\theta \\ y(\theta) &= \begin{cases} \sin\theta, & \text{if } \theta < \pi \\ \sqrt{2}\sin\theta, & \text{if } \theta \geq \pi \end{cases} \end{aligned} \tag{39}$$

The manipulator is a two-link planar 2R robot, with link lengths of 2 and 1. The rank-deficient manipulability constraint is defined by requiring the EE to have the capability of exerting a force along the tangent of the trajectory. A circular obstacle of radius $\frac{\sqrt{14}}{16} \approx 0.23$ is placed at $(\frac{1}{2}, 0)$. As such, with any non-zero clearance constraint to the obstacle, the manipulator is unable to reach the rightmost point $(\sqrt{2}, 0)$ on the curve.

In this case study, the assistive point is located at $(0, 1)$ where Joint 1 is $\frac{\pi}{2}$ rad. Obstacle avoidance prevents the manipulator from employing elbow-left configurations to cover the curve corresponding to the interval (approximately) $\theta \in (5.26, 2\pi)$, nor can it use elbow-right configurations to cover the curve corresponding to (approximately) $(0, 1.03)$. Even if manoeuvrability along all dimensions was not required, existing NCPP schemes [32] [33] could only consider purely non-singular cases. Hence, the valid singularity and a non-minimal surrounding region must be removed, leading to a section (around $\theta = \frac{\pi}{2}$) becoming uncoverable, as shown by Fig. 11(b).

To highlight the advantage of SNCPP, refer to Fig. 11(c). Assuming the curve has an analytic expression, whether θ_2 is greater or less than π is well-determined. Consequently, "colours" are always correctly assigned to configurations. Based on **Theorem 9**, the user can always designate an open interval surrounding the assistive point as an assistive cell, such as $(\frac{\pi}{2} - 0.01, \frac{\pi}{2} + 0.01)$, to transform the graph with singularity back to a normal cell-node graph. In the enumerative solving of the graph, a branch will be generated that enforces the assistive cell to connect "red" on the right-hand-side and "green" on the left-hand-side, ultimately leading to the optimal solution, without discontinuity, unlike the non-singular NCPP solution.

Next, we assume that the task-space contour is represented by discrete data with a 0.01 sample, $\theta = 0, 0.01, 0.02, ..., 6.27$

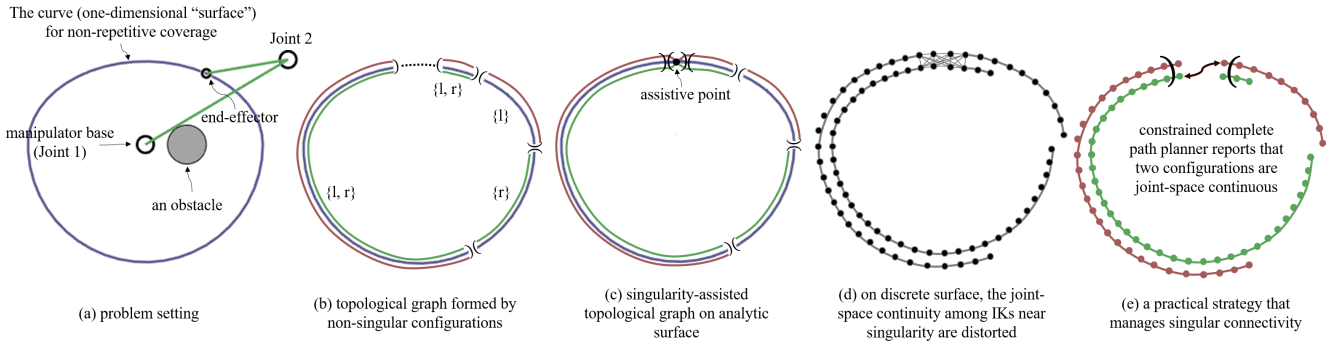

(a) problem setting (b) topological graph formed by non-singular configurations (c) singularity-assisted topological graph on analytic surface (d) on discrete surface, the joint-space continuity among IKs near singularity are distorted (e) a practical strategy that manages singular connectivity

Fig. 11. Demonstration of a non-repetitive curve visiting using a non-redundant 2 DoF manipulator.

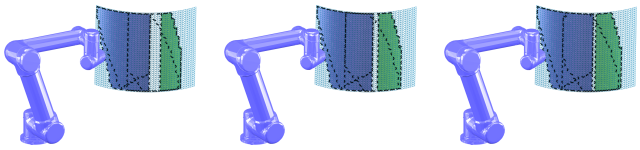

(a) Large ϵ_{regu} (b) Middle ϵ_{regu} (c) Small ϵ_{regu}

Fig. 12. Exclusion of configurations near a singularity conditioned by ϵ_{regu}.

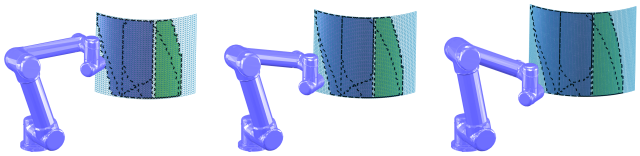

(a) Coarse Surface (b) Middle Surface (c) Fine Surface

Fig. 13. Interactions between ϵ_{cont}, ϵ_{regu} and discrete surface resolutions.

(a discrete sample approximation to $2\pi - 0.01$), where $\frac{\pi}{2}$ is not included in the set. In the absence of an assistive point, only the non-singular IK solutions are collected. Treating the problem as a normal NCPP problem with this representation is not applicable, as illustrated by Fig. 11(d). Section VII has proven that incorrect assignment of colour is inevitable: regardless of the value chosen for ϵ_{cont} to identify joint-space continuity, either two non-singularly connectable configurations are regarded as disconnectable, or two configurations that stay on opposite sides of the singularity are regarded as connectable. Adopting the proposed joint-space separation technique, the configurations unsuitable for coverage are separated, and specifically used for singular transition, whilst leaving other configurations for coverage, as depicted in Fig. 11(e). A constrained RRT planner has been utilised in all the examples shown in this work to find the path bridging cells, in this case the red configuration on the right-hand-side, and the green configuration on the left-hand-side, which constitutes the optimal path without discontinuity.

B. Performance under Various Parameter Settings

From the parameters introduced for the proposed solver, ϵ_{sing} and ϵ_{reso} correspond to intrinsic parameters–they are not manually set. ϵ_{cont} determines whether the topological graph

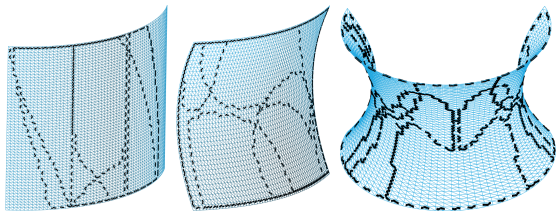

Fig. 14. Simulated object surfaces that include valid singular configurations (a generatrix of the cylinder, the central point of the saddle surface, and two points on the rotational surface slope, whose precise locations are however not captured by the discrete surface) when translational manipulability is considered.

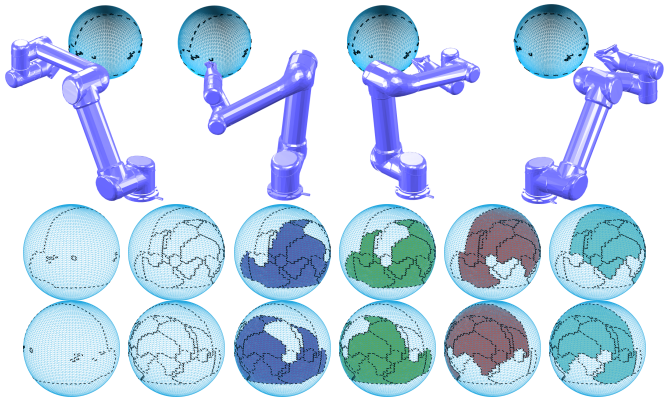

Fig. 15. Real-world experiment. Top: Four types of ill-conditioned configurations. Middle: (from left to right) topological graphs before and after joint-space separation, along with the coverable surface regions at four different non-singular configurations. Bottom: pictures of two non-singular configurations (wrist-flipped and wrist-unflipped), evidently not non-singularly connectable, yet both become part of the resultant SNCPP path (please refer to the supplementary video).

correctly models the SNCPP problem, being either correct or incorrect. Thus only ϵ_{regu} needs to be optimally set, and its choice is discussed in this section.

The first experiment–a support for the discrete case discussions in Section VIII–illustrates the optimal choice of ϵ_{regu} by running the SNCPP on a cylindrical surface. See Fig. 12 for an illustration with three different test cases. The generatrix of the cylinder is perpendicular to the ground, so the section

(a) (b) (c) (d) (e)

Fig. 16. Illustration of a manipulator motion near the singularity. The wrist has rotated for π rad, from a wrist-down configuration to a wrist-up configuration, but the EE pose changes little.

of the cylinder considered has the same valid singularity at every height as that of the equator of the sphere illustrated in Fig. 3. Hence there exist a line of assistive points that are singularly coverable, coinciding with the said generatrix. Given the same surface, coverage performance under different choices of ϵ_{regu} is visualised. In each testing case, ϵ_{cont} has been carefully selected such that the joint-space continuity among discrete configurations is correctly recognised. Large ϵ_{regu} excludes a sizeable area of non-singular configurations from the blue colour and green colour cells, leading to a wide gap between their coverage regions. Whilst in all cases a suitable ϵ_{cont} value can be drawn, the smallest ϵ_{regu} value is naturally the best choice amongst them. This leads to the second experiment, depicted in Fig. 13, where the amount of excluded configurations for singularity visiting and pose reconfiguration is examined. The same cylindrical surface has been modelled with different resolutions. In each testing case, ϵ_{regu} has been chosen to be the optimum, ensuring the existence of a valid ϵ_{cont} for correct graph construction. Results show that as the surface resolution grows, the region of excluded configurations becomes restricted to a single mesh column, the minimal configuration exclusion required by ϵ_{regu}, allowing for asymptotic optimal coverage as the precision of the discrete surface approaches infinity.

C. Algorithm Comparisons

The proposed coverage algorithm is compared with the classic boustrophedon [4] motion planner and the SOTA NCPP solution [33]. Neither of these algorithms is able to deal with singularities, so for a fair comparison, a small subset of near-singular valid configurations must be purposely removed. As such, the remaining configurations are all non-singular, forcibly introducing an additional lift-off by design, as there is a need to adopt a different colour for the coverage of the section. The algorithms are evaluated on four classic non-planar surfaces: a cylindrical surface, a saddle surface and a complex rotational surface in simulation, as well as a spherical object in a real-world setting. The resolution of each discrete surface is the same for all the algorithms applied. See Fig. 14 for illustration and Table. I for relative statistics. Results show that the proposed algorithm generates a continuous NCPP motion without discontinuity in all testing cases with minimal surface area left for singularity visiting. Also, it establishes the shortest task execution time and the least traversal motion

TABLE I
ALGORITHMS PERFORMANCE

Object	Alg.	Lift-offs	L_{Reconf}	L_{Joint}	L_{Task}	Time
Cylinder	boust [4]	53	409.16	491.87	170.26	1229.68
	[33]	2	7.12	74.82	18.99	187.05
	Ours	**0**	**1.87**	**69.57**	**18.22**	**173.93**
Saddle	boust [4]	10	56.02	218.52	16.15	546.30
	[33]	2	11.15	173.95	13.43	434.88
	Ours	**0**	**0.23**	**162.75**	**12.70**	**406.88**
Rotational Surface	boust [4]	37	295.81	455.33	68.22	1138.33
	[33]	4	29.57	172.86	20.77	432.15
	Ours	**0**	**1.50**	**147.30**	**10.06**	**368.25**
Sphere (real-world)	boust [4]	25	66.08	317.66	45.01	794.15
	[33]	2	2.48	235.02	30.54	587.55
	Ours	**0**	**0.58**	**233.12**	**30.30**	**582.80**

L_{Reconf}: Reconfiguration length (rad), derived by a constrained RRT.
L_{Joint}: L^2-norm Joint-space length (rad).
L_{Task}: Task-space length (m).
Time: Motion time (s).

in the work-cell (revealed by the shortest task-space travelling distance "L_{Task}" and the fact that the EE never leaves the surface). In contrast, the competing algorithms require a non-zero number of reconfiguration motions, and show longer "L_{Reconf}", "L_{Joint}", "L_{Task}", and "Time".

D. Real-world Experiment

A real-world experiment has been carried out to perform the coverage task in the frontal (reachable) section of a sphere. See Fig. 15. The existence of singularity is indicated by the non-local-bijective assignment of configuration colours, as depicted in Fig. 15 (middle part, leftmost). Multiple inverse kinematic configurations of a single mesh vertex are assigned the same colour, revealing the violation of local bijectivity. Additionally, tiny cells appeared, indicating incorrect joint-space connectivity identification. After setting ϵ_{regu}, the correct topological graph appears, depicted next to the incorrect graph. Four types of configurations distribute almost symmetrically, as the sphere is symmetric to the manipulator base. The full coverage involves pose reconfiguration from wrist-down to wrist-up configurations, imposing the traversal of a singularity, as shown in Fig. 16. The reader is referred to the supplementary video for further details and the full real-world motion.

X. CONCLUSION AND FUTURE WORK

This paper has proposed an algorithm to solve the non-redundant manipulator SNCPP task. Existing solutions to

solve the NCPP problem have purposely disregarded singular configurations. It is however shown that with the use of rank-deficient manipulability-related constraints, there may exist NCPP-suitable singularities whereby disjointed non-singular configuration sets can be bridged together, thus leveraging configuration continuity through singularities. SNCPP graph modelling for continuum surfaces has been formulated and analysed in detail first. It is proven that by enumerating all possible connectivities at each singularity, the problem can be transformed into a singularity-free topological graph which can be subsequently solved by existing NCPP solvers. Discussions on the practical strategy in dealing with the SNCPP on discrete surfaces have also been presented, and tested on simulated comparisons and a challenging real-world evaluation, supplemented by a video with further details to show the validity of the proposed scheme.

Currently, the enumerative solver for graphs without singularities is of exponential complexity. The additional enumerations presented by the introduction of each continuous set of assistive points will further exacerbate the enumerative space, hence the overall complexity remains exponential. Tractability and scalability are therefore areas to be considered in future work improvements.

XI. Acknowledgements

This work was supported in part by the National Nature Science Foundation of China under Grant 62173293, and in part by the National Key R&D Program of China under Grant 2023YFB4705000. This article is contribution n○ 1222 from AZTI, Marine Research, Basque Research and Technology Alliance (BRTA).

References

[1] E. U. Acar, H. Choset, A. A. Rizzi, P. N. Atkar, and D. Hull. Morse decompositions for coverage tasks. *Int. J. Robot. Res.*, 21(4):331–344, 2002.

[2] P. N. Atkar, H. Choset, and A. A. Rizzi. Towards optimal coverage of 2-dimensional surfaces embedded in $\mathbb{R}^3$: choice of start curve. In *IROS*, volume 4, pages 3581–3587. IEEE, 2003.

[3] S. Brown and S. L. Waslander. The constriction decomposition method for coverage path planning. In *IROS*, pages 3233–3238. IEEE, 2016.

[4] H. Choset. Coverage of known spaces: The boustrophedon cellular decomposition. *Auton. Robot.*, 9:247–253, 2000.

[5] E. Galceran and M. Carreras. A survey on coverage path planning for robotics. *Robot. Auton. Syst.*, 61(12):1258–1276, 2013.

[6] E. Glorieux, P. Franciosa, and D. Ceglarek. Coverage path planning with targetted viewpoint sampling for robotic free-form surface inspection. *Robot. Cim.-Int. Manuf.*, 61:101843, 2020.

[7] M. Hassan and D. Liu. A deformable spiral based algorithm to smooth coverage path planning for marine growth removal. In *IROS*, pages 1913–1918. IEEE, 2018.

[8] D. Heck, A. Saccon, N. V. D. Wouw, and H. Nijmeijer. Switched position-force tracking control of a manipulator interacting with a stiff environment. In *ACC*, pages 4832–4837, 2015.

[9] J. Hess, G. D. Tipaldi, and W. Burgard. Null space optimization for effective coverage of 3d surfaces using redundant manipulators. In *IROS*, pages 1923–1928. IEEE, 2012.

[10] W. Jing, J. Polden, C. F. Goh, M. Rajaraman, W. Lin, and K. Shimada. Sampling-based coverage motion planning for industrial inspection application with redundant robotic system. In *IROS*, pages 5211–5218. IEEE, 2017.

[11] D. Kaljaca, B. Vroegindeweij, and E. Van Henten. Coverage trajectory planning for a bush trimming robot arm. *J. Field Robot.*, 37(2):283–308, 2020.

[12] N. Karapetyan, K. Benson, C. McKinney, P. Taslakian, and I. Rekleitis. Efficient multi-robot coverage of a known environment. In *IROS*, pages 1846–1852. IEEE, 2017.

[13] M. Z. Li, Z. P. Lu, C. F. Sha, and L. Q. Huang. Trajectory generation of spray painting robot using point cloud slicing. *Appl. Mech. Mater.*, 44–47:1290–1294, 2011.

[14] B. Lin and X. Dong. Ship hull inspection: A survey. *Ocean Eng.*, 289:116281, 2023.

[15] K. M. Lynch and F. C. Park. *Modern robotics*. Cambridge University Press, 2017.

[16] R. K. Malhan, A. M. Kabir, B. Shah, and S. K. Gupta. Identifying feasible workpiece placement with respect to redundant manipulator for complex manufacturing tasks. In *ICRA*, pages 5585–5591. IEEE, 2019.

[17] S. McGovern and J. Xiao. A general approach for constrained robotic coverage path planning on 3d freeform surfaces. *IEEE T. Autom. Sci. Eng.*, pages 1–12, 2023.

[18] Y. Mei, Y. Lu, Y. C. Hu, and C. G. Lee. Energy-efficient motion planning for mobile robots. In *ICRA*, volume 5, pages 4344–4349, 2004.

[19] J. Molina, J. E. Solanes, L. Arnal, and J Tornero. On the detection of defects on specular car body surfaces. *Robot. Comput.-Integr. Manuf.*, 48:263–278, 2017.

[20] G. Oriolo and C. Mongillo. Motion planning for mobile manipulators along given end-effector paths. In *ICRA*, pages 2154–2160. IEEE, 2005.

[21] M. Ramesh, F. Imeson, B. Fidan, and S. L. Smith. Anytime replanning of robot coverage paths for partially unknown environments. *arXiv preprint arXiv:2311.17837*, 2023.

[22] S. S. M. Salehian and A. Billard. A dynamical-system-based approach for controlling robotic manipulators during noncontact/contact transitions. *IEEE Robot. Autom. Lett.*, 3(4):2738–2745, 2018.

[23] R. Seidel. A simple and fast incremental randomized algorithm for computing trapezoidal decompositions and for triangulating polygons. *Comput. Geom.*, 1(1):51–64, 1991.

[24] S. K. Singh. Motion planning and control of nonredundant manipulators at singularities. In *ICRA*, volume 2,

pages 487–492. IEEE, 1993.

[25] J. E. Solanes, L. Gracia, P. Munozbenavent, A. Esparza, J. Valls Miro, and J. Tornero. Adaptive robust control and admittance control for contact-driven robotic surface conditioning. *Robot. Comput.-Integr. Manuf.*, 54:115–132, 2018.

[26] S. Thakar, R. K. Malhan, P. M. Bhatt, and S. K. Gupta. Area-coverage planning for spray-based surface disinfection with a mobile manipulator. *Robot. Auton. Syst.*, 147: 103920, 2022.

[27] F. Tian, Z. Li, C. Lv, and G. Liu. Polishing pressure investigations of robot automatic polishing on curved surfaces. *Int J. Adv. Manuf. Tech.*, 87(1):639–646, 2016.

[28] F. Vigoriti, F. Ruggiero, V. Lippiello, and L. Villani. Tracking control of redundant manipulators with singularity-free orientation representation and null-space compliant behaviour. In *Human Friendly Robotics: 10th International Workshop*, pages 15–28, 2019.

[29] Y. Wen, D. J. Jaeger, and P. R. Pagilla. Uniform coverage tool path generation for robotic surface finishing of curved surfaces. *IEEE Robot. Autom. Lett.*, 7(2):4931–4938, 2022.

[30] C. Wu, C. Dai, X. Gong, Y. Liu, J. Wang, X. Gu, and C. Wang. Energy-efficient coverage path planning for general terrain surfaces. *IEEE Robot. Autom. Lett.*, 4(3): 2584–2591, 2019.

[31] X. Xie and L. Sun. Force control based robotic grinding system and application. In *WCICA*, pages 2552–2555, 2016.

[32] T. Yang, J. Valls Miro, Q. Lai, Y. Wang, and R. Xiong. Cellular decomposition for non-repetitive coverage task with minimum discontinuities. *IEEE/ASME T. Mech.*, pages 1698–1708, 2020.

[33] T. Yang, J. Valls Miro, Y. Wang, and R. Xiong. Non-revisiting coverage task with minimal discontinuities for non-redundant manipulators. In *RSS*, pages 1–8, 2020.

[34] T. Yang, J. Valls Miro, Y. Wang, and R. Xiong. Optimal object placement for minimum discontinuity non-revisiting coverage task. In *ICRA*, pages 8422–8428. IEEE, 2021.

[35] T. Yang, J. Valls Miro, Y. Wang, and R. Xiong. Optimal task-space tracking with minimum manipulator reconfiguration. *IEEE Robot. Autom. Lett.*, 7(2):5079–5086, 2022.

[36] T. Yang, J. Valls Miro, M. Nguyen, Y. Wang, and R. Xiong. Template-free nonrevisiting uniform coverage path planning on curved surfaces. *IEEE/ASME T. Mech.*, 28(4):1853–1861, 2023.

[37] T. Yang, J. Valls Miro, Y. Wang, and R. Xiong. An improved maximal continuity graph solver for non-redundant manipulator non-revisiting coverage. *IEEE T. Autom. Sci. Eng.*, Early Access, 2024. doi: 10.1109/TASE.2024.3400518.

[38] T. Yoshikawa. Manipulability of robotic mechanisms. *Int. J. Robot. Res.*, 4(2):3–9, 1985.

[39] T. Yoshikawa. Translational and rotational manipulability of robotic manipulators. In *IECON*, pages 1170–1175, 1991.